



Preparation of cetyltrimethylammonium bromide modified montmorillonite nanomaterial for adsorption of a textile dye

Murat Kıranşan^a, Reza Darvishi Cheshmeh Soltani^b, Aydin Hassani^{a,c}, Semra Karaca^{a,**}, Alireza Khataee^{d,*}

^a Department of Chemistry, Faculty of Science, Atatürk University, 25240 Erzurum, Turkey

^b Department of Environmental Health Engineering, School of Health, Arak University of Medical Sciences, Arak, Iran

^c Photochemical Nanosciences Laboratory, Department of Chemistry "G. Ciamician", University of Bologna, Via Selmi 2, 40126 Bologna, Italy

^d Research Laboratory of Advanced Water and Wastewater Treatment Processes, Department of Applied Chemistry, Faculty of Chemistry, University of Tabriz, Tabriz, Iran

ARTICLE INFO

Article history:

Received 27 February 2014

Received in revised form 26 May 2014

Accepted 16 June 2014

Available online 14 July 2014

Keywords:

Adsorption
Acid orange 7
Experimental design
Intercalation
Montmorillonite
Nano-clay

ABSTRACT

The main aim of this investigation was to evaluate the efficacy of the cetyltrimethylammonium bromide (CTAB) modified montmorillonite (MMT) nanomaterial for the adsorption of Acid orange 7 (AO7) as an anionic dye in aqueous solutions. The decolorization efficiency (%) was first increased from 52.74% to 94.08% with increasing cation exchange capacity (CEC) from 0.5 to 1.0 CEC and then decreased to 74.89% with increasing the amount of added CTAB to 1.5 CEC. Response surface methodology (RSM) based on central composite design (CCD) was used to evaluate the effect of various operational parameters on the adsorption of AO7. Predicted values of decolorization efficiency were found to be in good agreement with obtained experimental values ($R^2 = 0.9649$). The maximum decolorization efficiency was predicted to be 87.19% at an AO7 concentration of 49 mg/L, adsorbent dosage of 0.8 g/L, reaction time of 27 min and initial pH of 6. The results of isotherm study fit the Freundlich model ($R^2 > 0.9$). Moreover, the adsorption of AO7 onto modified MMT was increased with increasing temperature which could be explained by the endothermic nature of the adsorption process.

© 2014 Taiwan Institute of Chemical Engineers. Published by Elsevier B.V. All rights reserved.

1. Introduction

The presence of organic dyes in aqueous environments can cause harmful effects on human beings and aquatic life as a result of their toxicity. Moreover, discharging effluents containing organic dyes into receiving water results in preventing light diffusion into aqueous phase [1–3]. Various treatment technologies have been used for removing organic dyes from aqueous solutions including biological process, ultrafiltration, electrochemical degradation and advanced oxidation processes (AOPs). Already, colored wastewaters are usually treated by physical or chemical processes due to low biodegradability of organic dyes [1,2,4,5]. Among various physico-chemical processes, adsorption process has been considered as a promising and effective method for the decolorization of colored wastewater owing to its low cost,

insensitivity to toxic substances, simplicity and ease of operation irrespective of its high capacity for removing organic dyes [4,6,7]. Moreover, adsorption process results in the formation of no hazardous substances [4]. However, the application of available and effective alternative adsorbents such as clay derivatives is required because of the high regeneration cost of activated carbon, as the most widely used adsorbent, and increasing industrial effluents [6]. Among the studied clays for the adsorption of organic dyes, expandable layered silicates for instance montmorillonite (MMT) with negative charge have received much more attention, because they are available, relatively cheap, easily extracted, non-toxic and mechanically and chemically stable [6,8–10]. However, the application of pure MMT clay is not efficient for removing anionic organic dyes such as Acid orange 7 (AO7) from aqueous media; thus, chemical modification of pure MMT with an appropriate chemical agent would be favorable to reach suitable surface charge in order to increase adsorption capacity of the clay [11]. The modification of MMT surface by using cationic surface active substances such as cetyltrimethylammonium bromide (CTAB) can change its surface properties such as surface charge, hydrophobicity and cation exchange capacity [10,12]. Therefore, in

* Corresponding author. Tel.: +98 411 3393165; fax: +98 411 3340191.

** Corresponding author. Tel.: +90 442 2314435; fax: +90 442 2360948.

E-mail addresses: skaraca@atauni.edu.tr, semra_karaca@yahoo.com (S. Karaca), a_khataee@tabrizu.ac.ir, ar_khataee@yahoo.com (A. Khataee).

the present investigation, the adsorption of an anionic acid dye using MMT modified with CTAB was considered in aqueous solutions. The application of nano-sized MMT was considered because of particular surface characteristics of a nanostructured material along with its large surface area compared to its original size. To the best of our knowledge, there is no report on the application of CTAB modified nano-sized MMT for removing AO7 as an anionic dye from aqueous media. To vigorously evaluate the effect of various operational parameters including the dye concentration, adsorbent dosage, reaction time and initial pH on the adsorption of AO7 onto CTAB modified MMT nanomaterial, response surface methodology (RSM) based on central composite design (CCD) was used due to its advantages compared to the one-factor-at-a-time statistical approach [13–16]. RSM is an effective experimental design approach to determine the efficiency of an experimental system [17]. Using RSM, various parameters are simultaneously examined with a minimum number of experiments, which indicates that the study processed by RSM is less expensive and time consuming than the conventional strategy [13,18,19]. Additionally, the isotherm study was carried out to achieve a better understanding of the adsorptive characteristics of the CTAB modified MMT for subsequent use in full-scale applications.

2. Materials and methods

2.1. Chemicals

The MMT nano-clay was K-10 grade purchased from Sigma-Aldrich Co. (USA) with a surface area of 220–270 m²/g. The cation-exchange capacity (CEC) of the clay (60 meq/100 g) was determined by the ammonium acetate method [20,21]. All chemicals and reagents were of analytical grade purchased from Merck, Germany. The dye, acid orange 7, was purchased from Shimi Boyakhsaz Company, Iran and used as received. The specifications of the AO7 along with CTAB are given in Table 1.

2.2. Preparation of CTAB modified MMT nanomaterial

To synthesize surfactant modified MMT nanomaterial, 1 g MMT was first dispersed in 100 mL distilled water and stirred for 10 h at a stirring speed of 250 rpm to swell and to reach homogeneity. Then a desired amount of CTAB was slowly added. The concentrations of surfactants were 0.5, 1.0, 1.5 and 2.0 times CEC of pure MMT. The mixture was stirred for 1 h, then stirring was stopped and the resulting CTAB modified MMT was filtered and washed with distilled water for several times to remove excess salts, and then dried at 90 °C in an oven. The product was ground

and sieved using standard sieves to obtain chemically modified adsorbent [11,22,23]. The hypothetical simulating of the modification of MMT with CTAB is depicted in Fig. 1.

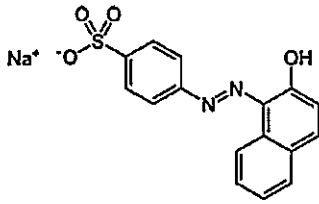
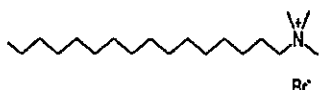
2.3. Experimental system and analysis

The adsorption experiments were performed using 100-mL glass-stoppered round-bottom flasks immersed in a thermostatic shaker bath as batch experimental reactors. The supernatant was withdrawn and centrifuged for 5 min at 6000 min⁻¹ to determine the final concentration of AO7 in the solution at the end of experimental run. The final concentration of AO7 was measured spectrophotometrically using a Varian Cary 100 UV at λ_{\max} of 485 nm. It was found that the supernatant from the adsorbent samples did not exhibit any absorbance at this wavelength. The calibration curve was very reproducible and linear over the concentration range used in this study. The amount of AO7 adsorbed was calculated from the difference between the concentrations in the solution before and after adsorption. Decolorization efficiency (%) of AO7 was calculated through Eq. (1):

$$\text{Decolorization efficiency (DE (\%))} = [1 - (C/C_0)] \times 100 \quad (1)$$

where C_0 and C are the dye concentration (mg/L) at time 0 and t , respectively [17,24]. A WTW inoLab pH meter (WTW Inc., Weilheim, Germany) was applied to measure the initial pH adjusted with concentrated HCl and NaOH solutions. Field emission scanning electron microscopy (FE-SEM) was conducted by a Mira microscope (Mira3, Tescan, Czech Republic) to study surface morphology of the adsorbent. XRD measurements of the raw and CTAB modified clay samples were performed using Rigaku 2200D/Max-IIIC (Rigaku Corporation, Tokyo, Japan). SEM images were further supported by energy dispersive X-ray (EDX) microanalysis to provide direct evidence for the purity, existence and distribution of specific elements in a solid sample. FT-IR spectra of the adsorbent samples before and after the adsorption of AO7 were run on a Perkin Elmer Model 1600 FT-IR spectrophotometer (USA) using KBr pellets. Each sample was finely ground with oven-dried spectroscopic grade KBr and pressed into a disc. All samples were dried at 120 °C in an oven to remove physisorbed water. Then, the spectra were recorded at wavenumber range between 400 and 4000 cm⁻¹. The point of zero charge (pH_{pzc}) of the modified MMT nanomaterial was measured using the method described by Bessekhouad et al. with some modifications [25]. In this approach, 500 mL 0.01 M NaCl was prepared and divided into five solutions with pH ranging from 3 to 10 adjusted by HCl and NaOH with suitable molarity. Hundred milligram adsorbent was added to each solution. Finally, the final pH of each solution was measured after 24 h and plotted against initial pH to determine

Table 1
Characteristics of acid orange 7 (AO7) and cetyltrimethylammonium bromide (CTAB).

C.I. name	Chemical structure	Molecular formula	M_w (g/mol)	pKa	λ_{\max} (nm)
Acid orange 7 (AO7)		C ₁₆ H ₁₁ N ₂ NaO ₄ S	350.32	11.4	485
Cetyltrimethylammonium bromide		(C ₁₆ H ₃₃)N(CH ₃) ₃ Br	364.45	-	-

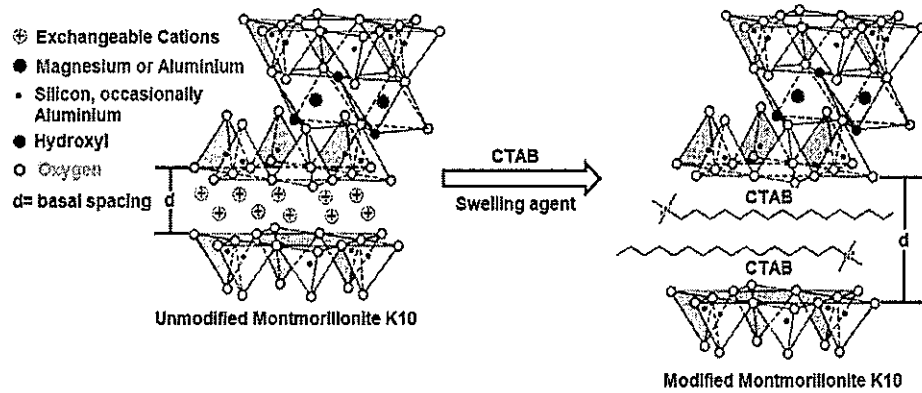


Fig. 1. A schematic flow diagram of the modification of MMT with CTAB.

pH_{zpc} of the adsorbent which is the crossing point of the line of final pH and initial pH. Zeta potentials of unmodified and modified MMT at natural pH were measured by using a Zeta Meter 3.0+ (Zeta-Meter, Inc., Staunton, VA, USA) at the unadjusted pHs.

2.4. Experimental design

Central composite design (CCD) was applied to carry out experimental design of the adsorption of AO7 on CTAB modified MMT nanomaterial. Design-Expert software was used for estimating DE (%) of AO7 and obtaining optimized operational parameters to achieve the maximum DE (%). Four main parameters influencing DE (%), including initial AO7 concentration (mg/L), adsorbent dosage (g/L), reaction time (min) and initial pH were chosen to perform an experimental design based on CCD. Prior to the experimental design, some pretests were carried out to reach a better understanding of the potential of the adsorbent for removing AO7 and to perform a reliable experimental design with justifiable ranges and levels of the operational parameters. Accordingly, the ranges and levels of the selected parameters are represented in Table 2. On the basis of the number of operational parameters, the number of experimental run was calculated through the following equation:

$$N = 2^k + 2k + x_0 \quad (2)$$

where N is the number of experiments, k is the number of parameters and x_0 is the number of central points, respectively. Therefore, the total number of experimental run was 31 ($k=4$, $x_0=7$). The selected parameters (X_i) were coded as x_i through Eq. (3):

$$x_i = (x_i - x_0) / \delta x \quad (3)$$

where x_0 and δx are the values of x_i at the center point and step change, respectively [26,27]. The coded parameters for axial points were calculated through Eq. (4):

$$\alpha = n_{fat}^{1/4} \quad (4)$$

Table 2
Ranges and levels of the experimental parameters for the adsorption of AO7 on CTAB-modified nano-MMT.

Run no.	Code	Parameter	Parameter level				
			-2 (α)	-1	0	+1	+2 (α)
1	X_1	Dye concentration (mg/L)	20	40	60	80	100
2	X_2	Adsorbent dosage (g/L)	0.1	0.3	0.5	0.7	0.9
3	X_3	Reaction time (min)	5	15	25	35	45
4	X_4	Initial pH	3	5	7	9	11

where n_{fat} is the number of assays of factorial design 2^4 [28]. The experimental data were fitted to a quadratic model, as shown in Eq. (5):

$$Y \text{ (predicted DE (\%))} = b_0 + b_1x_1 + b_2x_2 + b_3x_3 + b_4x_4 + b_{12}x_1x_2 + b_{13}x_1x_3 + b_{14}x_1x_4 + b_{23}x_2x_3 + b_{24}x_2x_4 + b_{34}x_3x_4 + b_{11}x_1^2 + b_{22}x_2^2 + b_{33}x_3^2 + b_{44}x_4^2 \quad (5)$$

where b_0 is constant (regression coefficients), x_1 , x_2 , x_3 and x_4 are the coded operational parameters; b_1 , b_2 , b_3 and b_4 are the linear effect terms; b_{11} , b_{22} , b_{33} and b_{44} are the quadratic effect terms; and b_{12} , b_{13} , b_{14} , b_{23} , b_{24} and b_{34} are the interaction effect terms [24].

3. Results and discussion

3.1. Adsorbent characteristics

Fig. 2 illustrates the XRD patterns of pure MMT and CTAB/MMT with different amounts of CTAB (0.5, 1.0, 1.5 and 2.0 CEC of MMT). A typical diffraction peak of pure MMT is placed at 7.1° , corresponding to a basal spacing of 1.21 nm. After intercalation

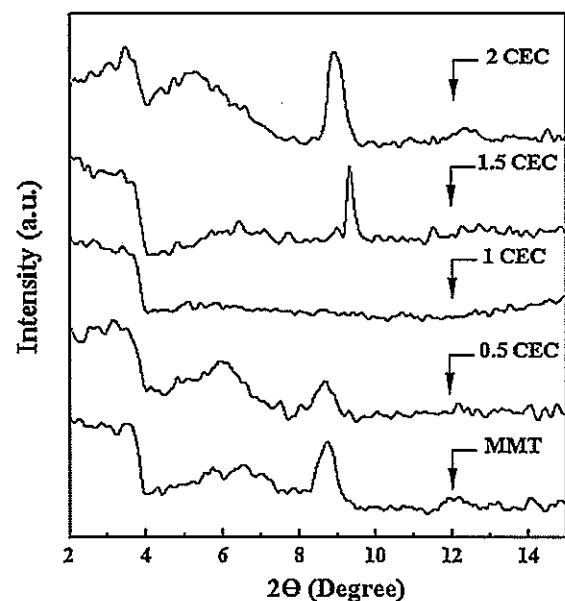


Fig. 2. XRD patterns of pure MMT and CTAB-modified MMT with various amounts of CTAB (0.5; 1.0; 1.5 and 2.0 CEC).

with CTAB, the position of this peak altered. The movement of the typical diffraction peak of pure MMT to lower angle (6.1°), responding to a basal spacing of 1.44 nm, indicates the formation of the intercalated nanostructure with CTAB content of 0.5 CEC. The intensity of the peak disappeared with further increasing of the amount of CTAB, implying the formation of the dominantly exfoliated nanostructure in CTAB/MMT for CEC of 1.0. With the increase of the concentration of swelling agent, the stack density of organic cations in the interlayer space increases and the arrangement of organic cations changes. The heterogeneity of charge on various layers may be the crucial factor for different arrangements coexisting [23]. This happening can be seen from 1.5 and 2.0 CEC of MMT, especially for 2.0 CEC.

SEM analysis was carried out to evaluate surface morphology of the unmodified and modified MMT and the results are depicted in Fig. 3. As shown, both unmodified and modified MMT had uneven structure with non-uniform size distribution. In the SEM image of MMT sample some phase separations and cracks are seen which like generally as a heterogeneous surface morphology. It can be also seen in Fig. 3(a) that pure MMT is comprised of fine particles, while the introduction of CTAB leads to large particles and coarse porous surface, which may be due to the penetration of dye molecules into the galleries of CTAB-MMT, resulting in an increase in the adsorption capacity of CTAB/MMT for the adsorption of AO7 (see Fig. 3(b)–(e)) [11,29]. Based on the EDX micrograph (Fig. 3(f)), the major portion of the modified MMT nanomaterial is composed of Si compounds, which are suitable for the adsorption of various organic pollutants such as organic dyes from aqueous solution. The weight percent (wt%) of Si, O, Al, C, Fe, Mg and K compounds within the adsorbent was 44.42, 32.50, 9.10, 8.46, 3.23, 1.57 and 0.70%, respectively. In addition to EDX analysis, FT-IR spectra of pure MMT, CTAB modified MMT nanomaterial, before and after the adsorption of AO7, were recorded in the wavenumber range between 400 and 4000 cm^{-1} (Fig. 4).

As shown in Fig. 4, the infrared spectra of modified MMT nanomaterial before and after the adsorption of dye show the strong bands at 2932 and 2854 cm^{-1} attributed to asymmetric and symmetric stretching vibrations of C–H groups. The lack of these peaks in the spectrum of pure MMT indicates the incorporation of the surfactant into the structure of MMT. In addition, a sharp peak located at 1472 cm^{-1} can be related to bending vibrations of NH_4^+ , supporting the intercalation of surfactant molecules between the silica layers. In the case of pure MMT, the band in the region of 950–1104 cm^{-1} (stretching vibration of Si–O group divided into a sharp band at 1059 cm^{-1} and a shoulder around 1104 cm^{-1}) attributed to perpendicular Si–O stretching. The band shape changed and its frequency shifted to lower wavenumber after the modification of MMT. The absorption band of –OH bending vibration of H_2O of MMT shifts significantly from 1650 cm^{-1} (pure MMT) to low frequency of 1640 cm^{-1} after the modification of MMT nanomaterial with CTAB, which indicates the removal of water molecules and the change in the hydrophobicity of MMT nanomaterial. On the other hand, CTAB produces more adsorption sites for enhancing the adsorption capacity of MMT nanomaterial for sequestering an anionic dye like AO7 [30]. This confirmed appropriate surficial structure of the adsorbent as well as successful modification of pure MMT with CTAB [30–36].

FT-IR spectrum of AO7 is presented in Fig. 4. As it is obvious, the major differences can be observed at 1624, 1599, 1572, 1555 and 1452 cm^{-1} , which are linked to C=C aromatic skeletal vibrations. The peak located at 1402 cm^{-1} can be assigned to O–H bending vibrations, while those located at 1198 cm^{-1} (shoulder) and 1304 cm^{-1} are due to the symmetric and asymmetric vibrations of the sulfonate groups, respectively. The strong bands at 1239, 1166, and 1042 cm^{-1} , attributed to S=O stretching, diminished after the adsorption. At the same time, the sharp peak at 1514 cm^{-1} ,

assigned to –N=N– stretching, reduced after the adsorption. The results indicated that the –N=N– and –SO₃ groups of AO7 are involved in the adsorption process. Furthermore, the peaks at 1505, 1447 and 1402 cm^{-1} , attributed to aromatic skeletal vibrations, have been shifted, broadened, and reduced after the adsorption. The bands at 830, 745, 702 cm^{-1} , assigned to the characteristic adsorption of aromatic skeletal groups, have been also reduced after the adsorption [31]. Moreover, the IR spectra of CTAB/MMT before and after the adsorption showed that the wide absorption band at 3435 cm^{-1} , corresponding to –OH stretching vibration of H_2O of MMT, broadened and strengthened after the adsorption. The absorption bands at 1640 cm^{-1} , assigned to the absorption band of –OH stretching vibration of H_2O of MMT, strengthened and shifted to lower wavenumber of 1636 cm^{-1} [31]. The results of IR analysis suggested that AO7 on CTAB/MMT is held by physical adsorption. It can be explained by the fact that the hydrophobic surface of modified MMT has more preference for the dissociated species of AO7 in aqueous solution. In addition, there is an electrostatic attraction between the cationic centers in modified MMT and the anionic SO₃[–] group in AO7 molecule. The van der Waals interaction between the phenyl ring of AO7 and –CH₂– group of modified MMT through hydrogen bonds can be another mechanism for the adsorption of AO7 onto CTAB-modified MMT.

3.2. Effect of the amount of CTAB on the adsorption capacity of modified MMT nanomaterial

To determine the optimum amount of CTAB for the chemical modification of MMT nanomaterial, four concentrations of CTAB were used for the modification to produce CECs of 0.5, 1.0, 1.5 and 2.0 CEC of pure MMT nanomaterial. For this set of experiments, initial AO7 concentration, adsorbent dosage and temperature were constant at 30 mg/L, 0.4 g/L and 298 K, respectively. Fig. 5 shows that the pure MMT nanomaterial is not efficient enough to remove AO7 from aqueous solutions (DE of 17.04%) as expected. As exhibited in Fig. 5, the DE (%) of AO7 was increased from 52.74% to 87.28% with increasing CTAB from 0.5 to 1.0 CEC, within a reaction time of 30 min. But increasing CTAB content to 1.5 and 2 CEC resulted in decreasing DE (%) to 74.89% and 79.63%, respectively. The surfactant orientation at interlayer galleries of clay particles depends on the surfactant loading [32]. It can be stated that the interactions between CTA⁺ ions and the negative centers on the montmorillonite surface occur through weak and electrostatic interactions. The decrease in DE after 1.0 CEC may be the result of increasing of the tendency of dye molecules to escape from the surface to bulk solution due to orientation of CTA⁺ ions in the basal spaces. To assess the effect of chemical modification on the surface characteristics of the adsorbent, zeta potential of the pure nano-MMT and modified MMT nanomaterial was measured. The zeta potential of pure MMT nanomaterial and CTAB modified MMT nanomaterial at 1.0 CEC was obtained to be –30.7 and 7.88 mV, respectively, indicating that the adsorption of dye molecules does not mainly occur through electrostatic interactions and also the presence of weak forces between the adsorbate molecules and adsorbent may be expected. Moreover, the pH_{pzc} of CTAB modified MMT nanomaterial at 1.0 CEC was obtained to be 4.5. Thus, organoclay nanomaterial carries negative charge on its surface and AO7 exists in anionic form resulting in no adsorption taking place on the adsorbent, as both have the same charge [33]. Therefore, enhanced adsorption of AO7 onto CTAB-modified MMT nanomaterial can be attributed to the interaction between AO7 and CTAB not surficial functional groups of the pure MMT nanomaterial. Overall, CTA⁺ is first attached firmly in the interlayer of MMT through electrostatic attraction with the negative surface charge of the MMT nanomaterial. Then, van der Waals attraction,

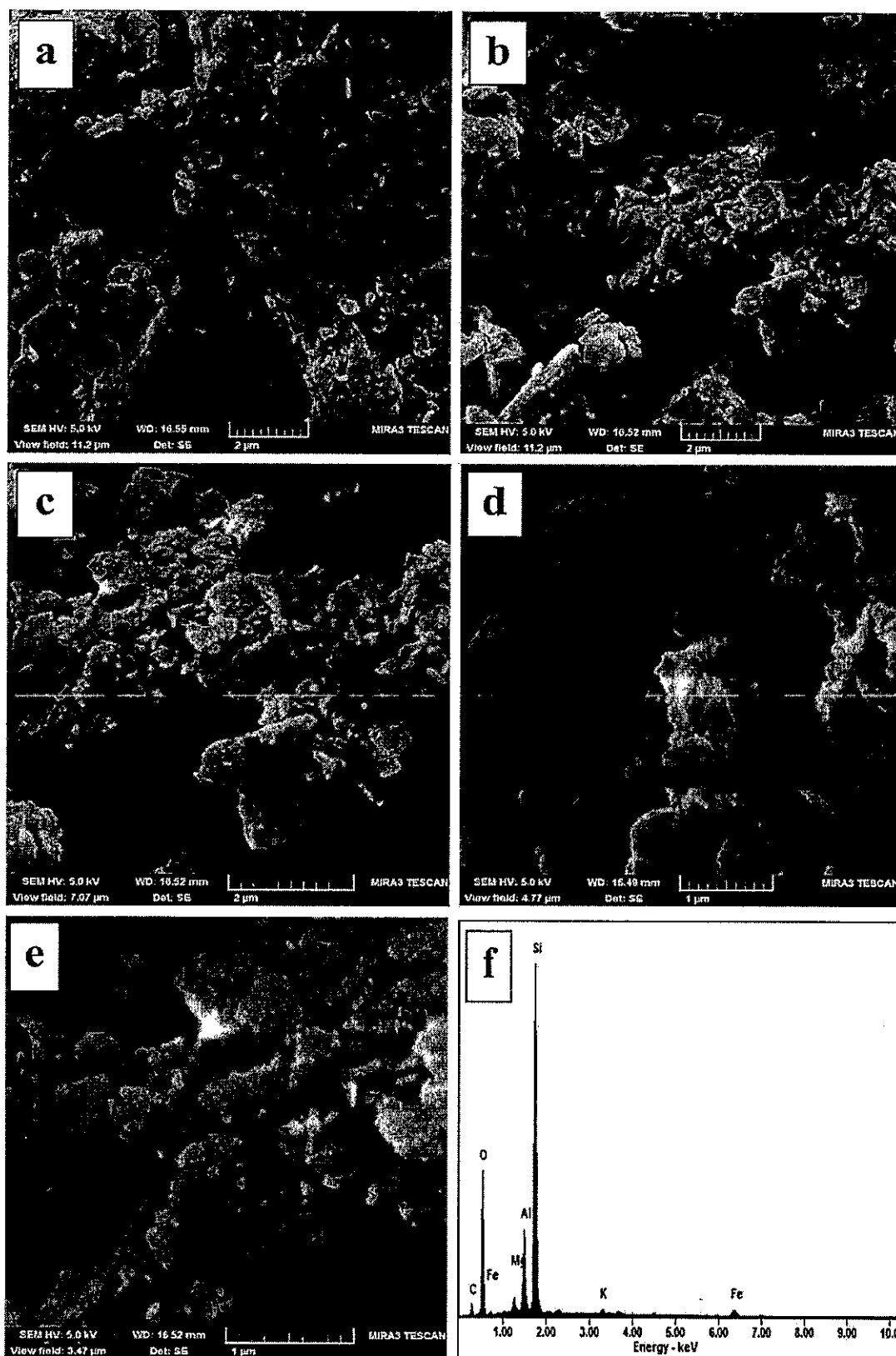


Fig. 3. SEM images of the pure MMT (a) and CTAB modified MMT (b–e) along with EDX micrograph of the modified MMT (f).

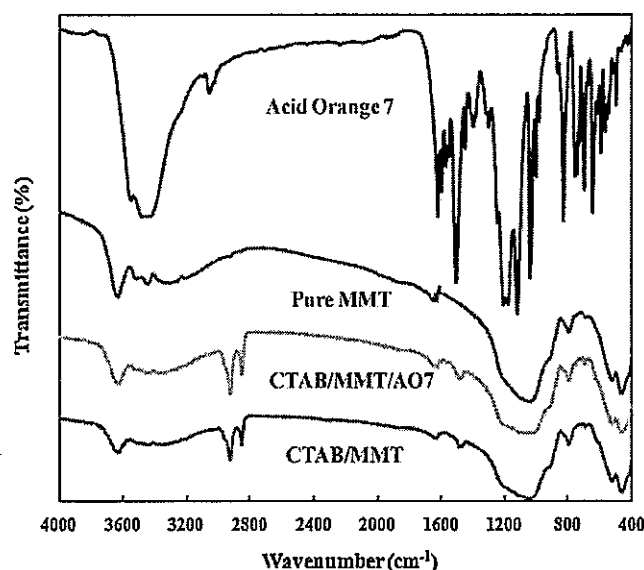


Fig. 4. FT-IR spectra of the AO7, pure MMT and CTAB modified MMT before and after the adsorption of AO7.

partly electrostatic interactions or hydrogen bonding interactions may be suggested to operate in such cases irrespective of the adsorption of AO7 as an anionic dye by anionic exchange with bromide ions of the CTAB molecules [31]. The following experiments were conducted with CTAB modified-MMT nanomaterial on 1.0 CEC of the pure MMT.

3.3. CCD results

The experiments were carried out and the obtained DE (%) for each experimental run was written down according to the experimental design accomplished by CCD. A mutual relationship

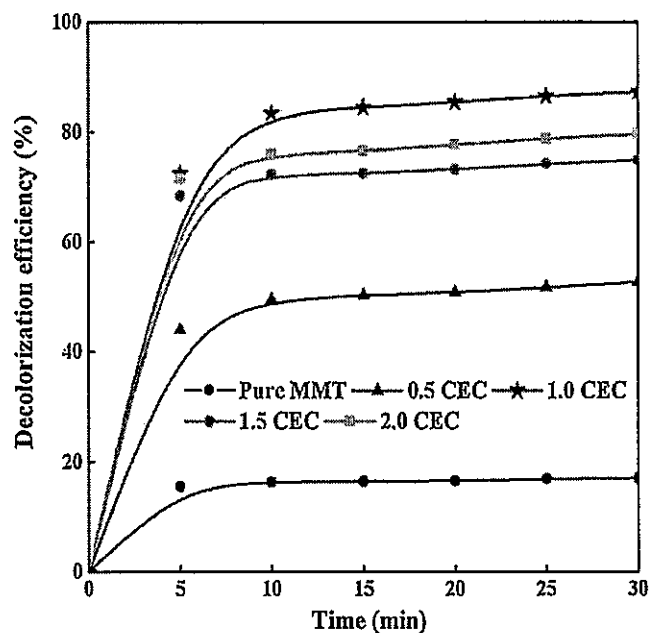


Fig. 5. Effect of the amount of CTAB in terms of cation exchange capacity on the decolorization efficiency of AO7.

between the response (DE (%)) and the operational parameters was obtained, which is shown in Eq. (6):

$$Y \text{ (DE (\%))} = 58.96 - 10.16x_1 + 11.86x_2 + 1.69x_3 - 1.24x_4 \\ - 2.17x_1x_2 + 0.46x_1x_3 + 1.28x_1x_4 + 1.25x_2x_3 \\ - 1.50x_2x_4 - 0.053x_3x_4 + 1.10x_1^2 - 1.10x_2^2 \\ - 1.13x_3^2 + 1.33x_4^2 \quad (6)$$

The obtained quadratic model equation was used to predict the optimum value for each parameter within the specified range to achieve maximum DE (%). Moreover, it would be beneficial to clarify the interaction effects between various operational parameters [17]. According to Eq. (6), the experimental paths and corresponding experimental conditions together with experimental and predicted DE (%) is displayed in Table 3. One of the most important approaches to evaluate the suitability and significance of the statistical model is performing analysis of variance (ANOVA) [27]; thus, ANOVA was carried out for the adsorption of AO7 on CTAB modified MMT nanomaterial and the results are shown in Table 4. On the basis of the obtained high correlation coefficient ($R^2 = 0.9649$), which indicates a good agreement between the predicted and experimental results for DE (%), the significance of the applied model was favorable (Fig. 6(a)). The correlation coefficient indicated that the model does not explain only 3.51% of the variations. The value of R^2 was calculated through Eq. (7):

$$R^2 = 1 - (SS_{\text{residual}}/SS_{\text{model}} - SS_{\text{residual}}) \quad (7)$$

where SS is the sum of the square. Furthermore, the adjusted R^2 rectifies the value of R^2 for the sample size and the number of terms using the degrees of freedom on its computations. Adjusted R^2 was calculated via Eq. (8):

$$\text{Adjusted } R^2 = 1 - ((n-1)/(n-p)(1-R^2)) \quad (8)$$

where n is the number of experiments and p is the number of predictors in the applied model [34]. A smaller obtained adjusted R^2 compared to the R^2 can be due to the presence of many terms in the applied model together with not very large sample size [35]. But adjusted R^2 was close to the value of R^2 , indicating a good fitness between the predicted and experimental DE (%). A similar result was reported by Singh and coworkers during optimization of the adsorption of a textile dye on a magnetic nanocomposite using RSM based on CCD [26]. As depicted in Table 4, the high value obtained for adequate precision (22.42) along with low value for the coefficient of variation ($CV = 6.41\%$) demonstrated a good reliability for the experiments. In addition, the significance of the model can be assessed by the obtained residuals. The evaluation of the residuals can be an appropriate tool to exhibit how well the model satisfies the assumptions of the ANOVA [17]. The residual for each experimental run was calculated via determining the difference between the experimental and the predicted DE (%) (Table 3). Fig. 6(b) shows the plot of normal (%) probability versus residuals. As depicted in Fig. 6(b), the obtained data points are on a relatively straight trend line with no obvious dispersal, which suggests normal distribution of the residuals. The residuals versus the predicted DE (%) and the run number were illustrated in Fig. 6(c) and (d), respectively, demonstrating a random dispersal of the residuals towards predicted DE (%) and run number.

Finally, the significance of the model was verified by the obtained F -value and p -value for the model terms. The larger the quantity of the F -value and smaller p -value, the more significant the corresponding coefficient [14]. The p -value less than 0.05 and greater than 0.1 imply that the model term is significant and not significant, respectively. Thus, the obtained F -value of 31.39 and the p -value of <0.0001 indicated the suitability and adequacy of

Table 3
Experimental and predicted results for the adsorption of AO7 on CTAB-modified nano-MMT optimized by CCD.

Run no.	Coded parameters				Actual parameters				Decolorization efficiency (%)		
	X ₁	X ₂	X ₃	X ₄	X ₁	X ₂	X ₃	X ₄	Experimental	Predicted	Residuals
1	0	0	+2	0	60	0.5	45	7	61.70	57.82	3.880
2	+2	0	0	0	100	0.5	25	7	43.60	43.02	0.580
3	-1	+1	+1	+1	40	0.7	35	9	82.00	81.76	0.240
4	0	0	0	0	60	0.5	25	7	57.44	58.96	-1.52
5	+1	-1	+1	-1	80	0.3	35	5	37.27	38.71	-1.44
6	0	0	0	0	60	0.5	25	7	56.95	58.96	-2.01
7	+1	+1	-1	+1	80	0.7	15	9	52.84	53.88	-1.04
8	-1	-1	+1	+1	40	0.3	35	9	51.79	54.20	-2.41
9	+1	-1	-1	-1	80	0.3	15	5	34.42	36.82	-2.40
10	0	0	0	0	60	0.5	25	7	55.15	58.96	-3.81
11	-2	0	0	0	20	0.5	25	7	85.88	83.67	2.210
12	0	0	0	-2	60	0.5	25	3	67.78	66.76	1.020
13	-1	-1	-1	+1	40	0.3	15	9	51.75	54.36	-2.61
14	+1	-1	+1	+1	80	0.3	35	9	41.58	41.69	-0.11
15	-1	+1	-1	+1	40	0.7	15	9	77.71	76.91	0.800
16	0	0	0	+2	60	0.5	25	11	63.59	61.82	1.770
17	0	+1	0	0	60	0.9	25	7	79.88	78.28	1.600
18	0	0	0	0	60	0.5	25	7	55.82	58.96	-3.14
19	-1	-1	+1	-1	40	0.3	35	5	55.22	56.33	-1.11
20	0	0	0	0	60	0.5	25	7	60.86	58.96	1.900
21	+1	+1	+1	+1	80	0.7	35	9	57.20	60.57	-3.37
22	+1	-1	-1	+1	80	0.3	15	9	42.19	40.02	2.170
23	0	-2	0	0	60	0.1	25	7	32.03	30.84	1.190
24	+1	+1	+1	-1	80	0.7	35	5	64.05	63.60	0.450
25	0	0	0	0	60	0.5	25	7	57.48	58.96	-1.48
26	0	0	-2	0	60	0.5	5	7	49.98	51.07	-1.09
27	+1	+1	-1	-1	80	0.7	15	5	58.47	56.69	1.780
28	-1	+1	-1	-1	40	0.7	15	5	82.80	84.84	-2.04
29	-1	+1	+1	-1	40	0.7	35	5	87.10	89.91	-2.81
30	-1	-1	-1	-1	40	0.3	15	5	59.02	56.28	2.740
31	0	0	0	0	60	0.5	25	7	69.00	58.96	10.04

the model to describe the adsorption of AO7 on CTAB modified MMT nanomaterial (Table 4). The "Lack of Fit *F*-value" of 0.40 implies that the Lack of Fit is not significant, which is desirable (Table 4). Moreover, the obtained *F*- and *p*-value for each operational parameter can be used as efficient tools to evaluate the importance of each operational parameter against the other parameters [14,16].

According to Table 5, the adsorbent dosage (x_2) produces the largest effect on DE (%) (*F*-value = 235.41 and *p*-value < 0.0001), while the initial pH (x_4) (*F*-value = 2.56 and *p*-value = 0.1293) produces the least effect on DE (%). Among various interactive effects between studied parameters, the interactive effect of initial AO7 concentration and adsorbent dosage (*F*-value = 5.26 and *p*-value < 0.0357) produced the largest effect on DE (%).

3.4. Interactive effect of various operational parameters

The application of three-dimensional (3-D) response surface graph and corresponding contour graph was considered to specify the interactive effects of studied operational parameters. In this manner, 3-D surface graph and contour graph of two different operational parameters were depicted, while the other two parameters were constant. This can be helpful to understand both

the main and the interactive effects of two independent parameters [17,26].

3.4.1. Interactive effect of initial AO7 concentration and reaction time

As it is obvious from Fig. 7, increasing the initial AO7 concentration from 20 to 100 mg/L led to an evident drop in DE (%), while increasing elapsed time caused a gentle increase in DE (%) at constant adsorbent dosage of 0.5 g/L and initial pH of 7. A fast adsorption is predictable for initial stages of the process, while reaching equilibrium results in a slower adsorption [11,33]. Similar result was reported by Sharma et al. in the case of the adsorption of Acid Red 151 processed by CCD [17]. The lower DE (%) of AO7 at high initial dye concentration may be due to low number of vacant adsorption sites available for adsorbing dye molecules which results in decreasing DE (%) of AO7.

3.4.2. Interactive effect of adsorbent dosage and reaction time

By keeping the initial pH and dye concentration constant, the interactive effect of adsorbent dosage and reaction time was depicted in Fig. 8. As shown, an increase in adsorbent dosage resulted in a sharp increase in DE (%), indicating that the adsorbent dosage produces a major effect on DE (%). It confirms with the higher obtained value of *F*-value for the adsorbent dosage compared

Table 4
Analysis of variance (ANOVA) for the adsorption of AO7 on CTAB-modified nano-MMT.

Source	Sum of squares	Degree of freedom	Mean square	<i>F</i> -value	<i>p</i> -value	
Regression	6300.68	14	450.05	31.39	0.0001	Significant
Residuals	229.43	16	14.34			
Lack of Fit	92.10	10	9.21	0.40	0.9023	Not significant
Pure error	137.33	6	22.89			
Total	6530.11	30				

$R^2 = 0.9649$, adjusted $R^2 = 0.9341$, adequate precision = 22.42, coefficient of variation (CV) = 6.41 (%).

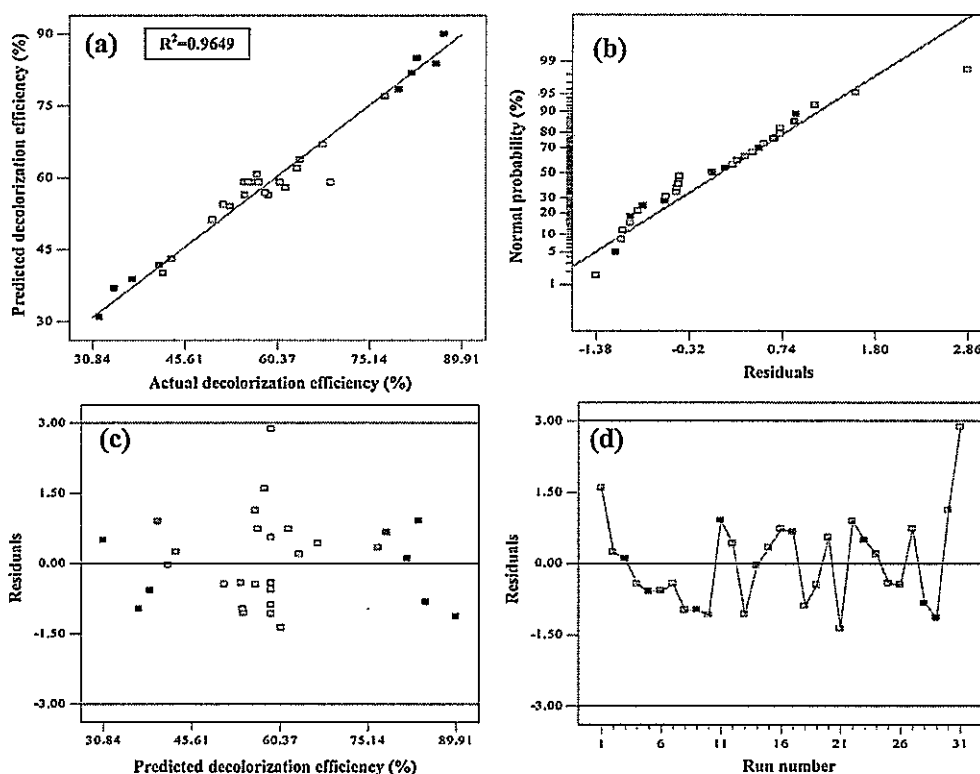


Fig. 6. The plot of predicted versus experimental decolorization efficiency (a) and corresponding residual plots (b–d).

to the other parameters (Table 5). But, similar to Fig. 7, increasing reaction time resulted in an insignificant increase in DE (%). The reason for this behavior may be the fact that increasing adsorbent dosage gives more surface area and more binding sites for the adsorption of the dye onto the adsorbent [24]. A similar result has been reported for the adsorption of an anionic dye by modified-KSF-montmorillonite [8]. As depicted in Table 5, *F*-value of reaction time was obtained to be 4.75, which was lower than that of obtained for initial AO7 concentration or adsorbent dosage.

3.4.3. Interactive effect of initial pH and the other operational parameters

Three-D response surface plot and corresponding contour plot of the interactive effect of the initial pH and initial AO7

Table 5
Estimated regression coefficient and corresponding *F*- and *p*-values obtained during central composite design for the adsorption of AO7 on CTAB-modified nano-MMT.

Coefficient	Coefficient estimate	Standard error	<i>F</i> -value	<i>p</i> -Value
x_0	58.96	1.43	31.39	0.0001
x_1	-10.16	0.77	172.90	0.0001
x_2	11.86	0.77	235.41	0.0001
x_3	1.69	0.77	4.75	0.0445
x_4	-1.24	0.77	2.56	0.1293
x_{12}	-2.17	0.95	5.26	0.0357
x_{13}	0.46	0.95	0.24	0.6341
x_{14}	1.28	0.95	1.83	0.1949
x_{23}	1.25	0.95	1.75	0.2042
x_{24}	-1.50	0.95	2.52	0.1319
x_{34}	-0.053	0.95	0.003	0.9559
x_{11}	1.10	0.71	2.40	0.1409
x_{22}	-1.10	0.71	2.41	0.1402
x_{33}	-1.13	0.71	2.54	0.1308
x_{44}	1.33	0.71	3.55	0.0780

concentration are shown in Fig. 9(a) and (b), respectively. Overall, the plots exhibited that decreasing initial pH, with respect to neutral or basic values, resulted in high increase in DE (%). This can be confirmed by the negative value of "coefficient estimate" for the initial pH (Table 5), implying that decreasing initial pH causes increase in DE (%). A similar behavior has been reported by Zohra et al. in the case of the adsorption of Direct Red 2 on CTAB intercalated bentonite [33]. The pH of the solution influences the surface charge and the dissociation of the functional groups of the adsorbent along with the degree of ionization of the adsorbate [8]. As can be observed in Fig. 9, the removal of AO7 was favored in acidic conditions (pH 3–5), reached an optimum around at pH 5 and slightly decreased at high pH. These results confirm the great influence of pH on AO7 adsorption by modified clay which already was evidenced in previous studies [36]. The pH_{zpc} value for modified-clay was determined 4.5. This value confirms the ranges of optimal pH values for dye removal from aqueous solutions. The pH_{zpc} of adsorbent indicated that the surface of adsorbent is positively charged at pH less than 4.5 and negatively charge at pH values above 4.5. At pH 3, a significantly high electrostatic attraction exists between negatively charged anionic AO7 and the positively charged surface of the adsorbent because of the protonation of adsorbent surface. As the pH of the system increases, the number of negatively charged sites increased due to deprotonation of adsorbent surface, which can adversely affect the adsorption of anionic dyes because of the electrostatic repulsion [8,37]. Also, increasing pH values leads to increasing the amount of OH^- ions competing with anionic dye for the adsorption onto CTAB modified MMT [31,38]. As illustrated in Fig. 9(c) and (d), unlike adsorbent dosage, the effect of initial pH on the adsorption was insignificant. As depicted, the effect of adsorbent dosage was higher than that of initial pH in which increasing the adsorbent dosage caused a rapid increase in DE (%). As shown in Table 5, this result can be proven by the obtained

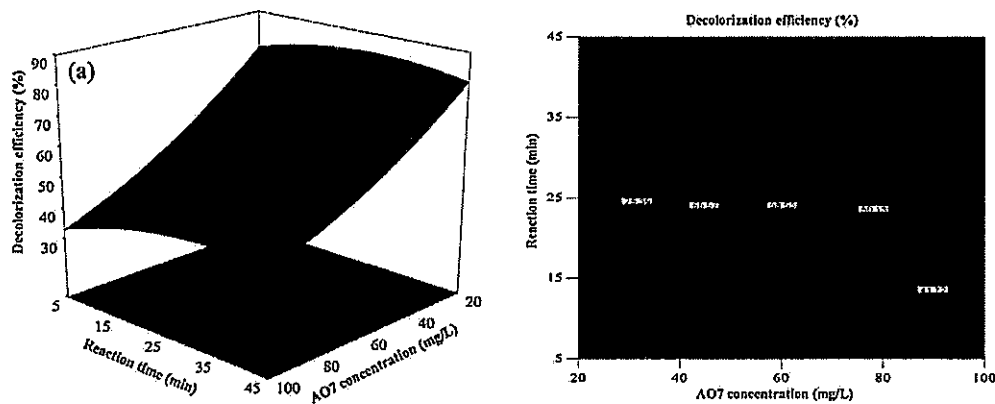


Fig. 7. The response surface plot (a) and corresponding counter plot (b) for the adsorption of AO7 as the function of initial dye concentration (mg/L) and reaction time (min).

smaller F -value for the initial pH in comparison with the other parameters.

3.5. Optimization

The numerical optimization was selected to determine desirable values for each parameter to reach the maximum DE (%). The possible ranges that can be selected for the response (DE (%)) include, maximum, minimum, equal, target or none. Whereas each input parameter was given full range. The response (DE (%)) was designed to the maximum value. So, the maximum DE (%) was 87.19% at an initial AO7 concentration of 49 mg/L, adsorbent dosage of 0.8 g/L, reaction time of 27 min and initial pH of 6. To validate the obtained results, additional experiments were carried out under optimum operational parameters to confirm predicted DE (%). The experimental value for DE (%) was obtained to be 86.63%, which is very close to the predicted DE (%), indicating the suitability and accuracy of the applied model for predicting DE (%) of AO7 under different operational conditions.

3.6. Effects of temperature

Temperature is an important parameter for the adsorption process. A plot of the AO7 uptake as a function of temperature (293, 313 and 333 K) is shown in Fig. 10. The results reveal that decolorization efficiency increases with increasing temperature. The adsorption of dye at high temperatures was found to be greater than that at a lower temperature showing that this process is endothermic [39]. This may be a result of increase in the mobility

of the dye with increasing temperature [40]. An increasing number of molecules may also acquire sufficient energy to undergo an interaction with active sites at the surface. Furthermore, increasing temperature may produce a swelling effect within the internal structure of the CTAB modified clay enabling large dye to penetrate further [41]. Bouberka et al. have reported that the amount of yellow 4GL (acid dye) adsorbed on modified clays increases with the increasing of temperature from 313 to 323 K [42]. Hameed et al. also have reported that the adsorption capacity of activated palm ash for acid green 25 at 30, 40, and 50 °C increase with increasing the temperature [43].

The thermodynamic parameters such as change in standard free energy (ΔG), enthalpy (ΔH) and entropy (ΔS) were determined by through Eqs. (9) and (10):

$$\ln K_c = \frac{\Delta S}{R} - \frac{\Delta H}{RT} \quad (9)$$

$$\Delta G_{\text{ads}} = \Delta H_{\text{ads}} - T\Delta S_{\text{ads}} \quad (10)$$

where R (8.314 J/mol K) is the ideal gas constant, T (K) the absolute temperature (K) and K_c (L/g) is the standard thermodynamic equilibrium constant defined by q_e/C_e . By plotting a graph of $\ln K_c$ versus $1/T$ (figure not shown) the values ΔH and ΔS can be estimated from the slopes and intercepts. The negative values of ΔG and positive ΔH indicates that the AO7 dye adsorption process is a spontaneous and an endothermic (Table 6). The positive value of ΔS suggests increased randomness at the solid/solution interface occurs in the internal structure of the adsorption of AO7 dye onto CTAB modified clay [44]. It is accepted that if

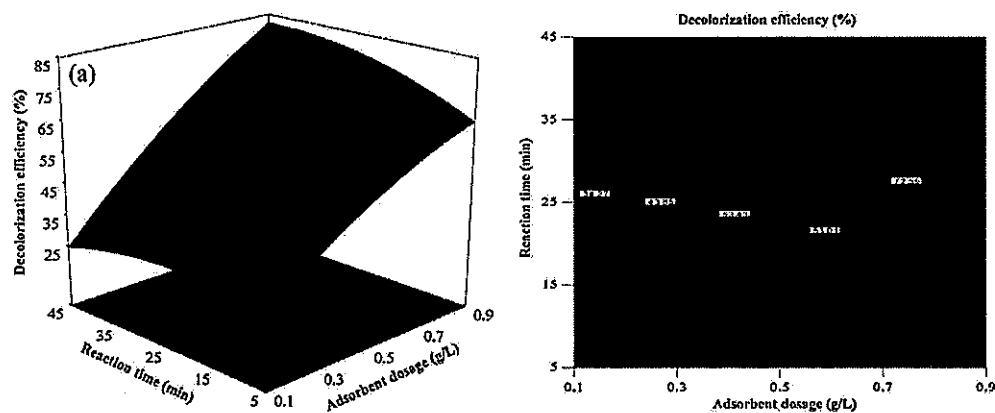


Fig. 8. The response surface plot (a) and corresponding counter plot (b) for the adsorption of AO7 as the function of adsorbent dosage (g/L) and reaction time (min).

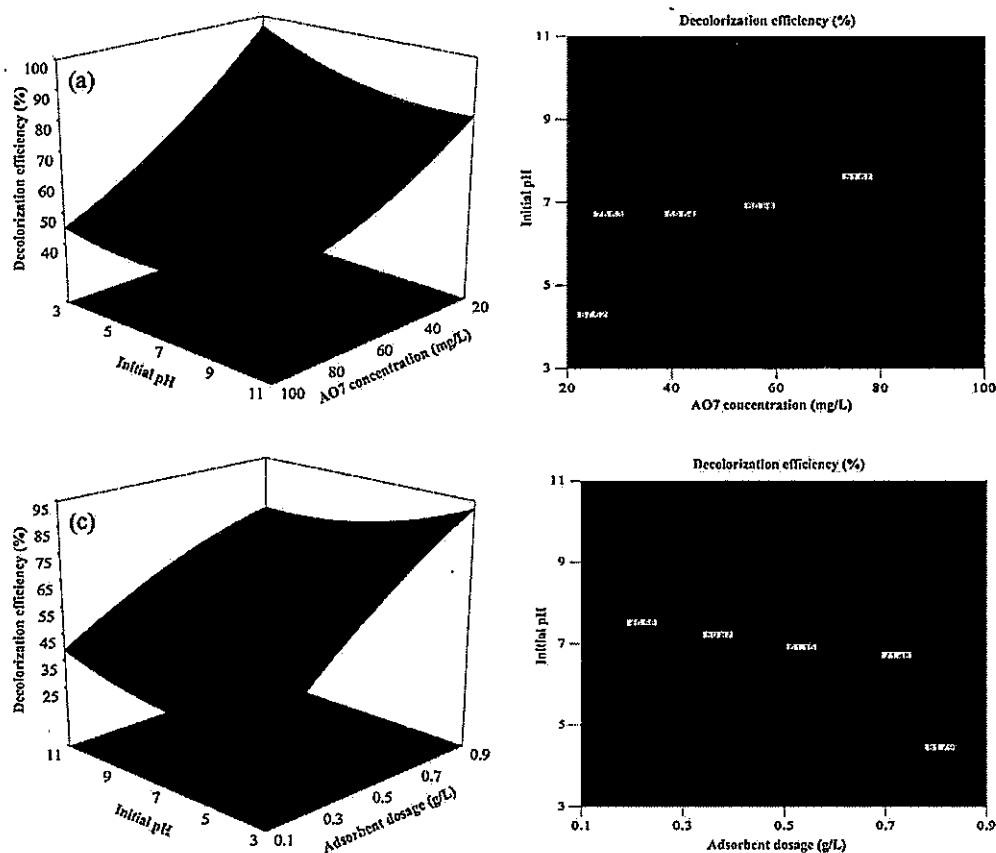


Fig. 9. The response surface plot and corresponding counter plot for the interactive effect of initial pH and initial dye concentration (a and b) and adsorbent dosage (c and d).

magnitude of enthalpy change is less than 84 kJ/mol, adsorption process occurs physically. However chemisorption takes place in the range from 84 to 420 kJ/mol. The adsorption behavior of molecules in the solid–liquid system was determined by a combination of two processes [45]: (i) the desorption of the molecules of solvent previously adsorbed, and (ii) the adsorption of adsorbate species. For the adsorption of AO7 dye molecules on

CTAB/MMT nanomaterial, more than one water molecule should be replaced due to its large molecular size and decreasing of surface energy. This phenomena might have occurred in the endothermicity of the adsorption process. The magnitude of enthalpy change (+27.54 kJ/mol) indicated that the adsorption of AO7 onto CTAB-modified MMT is physical in nature [45]. This is in agreement with the results of adsorption isotherm study as follows.

3.7. Adsorption isotherms

In order to determine the mechanism of the adsorption of AO7 on CTAB modified MMT at 293, 313 and 333 K, the experimental data were applied to the Langmuir, BET, Freundlich, Temkin, Dubinin–Radukevisch (D–R), Halsey, Harkins–Jura, Smith and Henderson isotherm models. The constant isotherm parameters were calculated by regression using the linear form of the isotherm equations and SPSS 10.0 software. The results of isotherm study are given in Table 7. The results did not fit the Langmuir and BET isotherm models, indicating no strong interactions between the adsorbent and adsorbate molecules [46]. The Freundlich

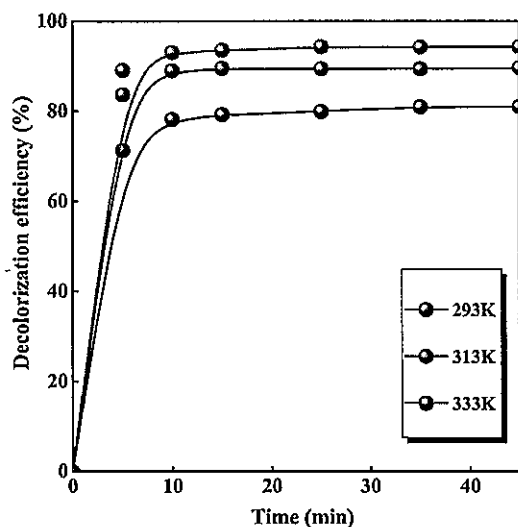


Fig. 10. Experimental isotherm of AO7 adsorbed onto CTAB modified MMT at different temperatures.

Table 6
Thermodynamic parameters of AO7 dye adsorption on CTAB modified nano-MMT.

Temperature (K)	Thermodynamic parameters		
	ΔG (kJ/mol)	ΔH (kJ/mol)	ΔS (kJ/mol K)
293	-43.95	27.54	0.056
313	-45.07		
333	-46.20		

Table 7
The results of isotherm study for the adsorption of AO7 onto CTAB-modified nano-MMT.

Isotherm models	Equation	Parameters	293 K	313 K	333 K
Langmuir	$C/q = 1/kq_m + (1/q_m)C$	q_m	–	–	–
		k	–	–	–
		R^2	0.2922	0.2615	0.7072
Freundlich	$\ln q = \ln k + n \ln C$	n	1.3765	1.5015	0.6893
		k	1.7137	2.1737	18.6622
		R^2	0.9404	0.9689	0.9689
BET	$C/q(1 - C) = 1/(q_m k) + [(k - 1/q_m k)]C$	q_m	–188.736	–106.388	–117.64
		k	–1.432	–3.357	17
		R^2	0.3769	0.6284	0.6819
Dubinin–Radukevišch	$\ln q = K\varepsilon^2 + \ln q_{DR}$	K	–4.9883	–4.1668	–1.2211
		q_{DR}	0.1638	6.3885	1.3412
		R_2	0.9313	0.9761	0.9244
		E	0.3165	0.3464	0.6398
Halsey	$\ln q = (1/n)\ln k - (1/n)\ln[\ln(1/C)]$	n	0.2964	0.2457	0.4027
		k	1.7499	2.1129	2.3781
		R^2	0.9299	0.9524	0.9373
Harkins–Jura	$1/q^2 = (B/A) - (1/A)\log C$	B	–0.8970	–1.036	–1.2143
		A	0.0105	0.0113	0.0305
		R^2	0.8801	0.8455	0.9203
Smith	$q = W_b - W \ln(1 - C)$	W	4.811	7.506	8.5192
		W_b	–0.0899	–0.1283	0.1254
		R^2	0.92	0.9587	0.9116
Henderson	$\ln[-\ln(1 - C)] = \ln k + n \ln q$	n	0.7145	0.6673	1.3825
		k	0.1994	0.1330	0.1097
		R^2	0.9398	0.9677	0.9394
Temkin	$q_e = (RT/b_T)\ln a_T + (RT/b_T)\ln C_e$	b_T	5369.19	4561.80	9297.71
		a_T	26.57	32.91	179.34
		R^2	0.883	0.944	0.8633

isotherm is an empirical equation that can be used for the heterogeneous adsorptive sites with interaction between the adsorbed molecules onto surface of the adsorbent [47]. As shown in Table 7, high R^2 values were obtained for Freundlich isotherm model for all studied temperatures. Moreover, the values of k (a measure of adsorbent capacity) and n (a measure of the intensity of adsorption) for the adsorption of AO7 onto CTAB modified MMT were increased with the increase in temperature. This suggests endothermic nature of the adsorption process. The results of Halsey, Harkins–Jura, Smith and Henderson isotherm models for the adsorption of AO7 onto CTAB modified MMT at different temperatures are given in Table 7. As exhibited in Table 7, the values of the correlation coefficients (R^2) indicate that all of the above-mentioned models fit the adsorption of AO7 onto CTAB modified MMT ($R^2 > 0.91$), except for Harkins–Jura model at 293 and 313 K ($0.8 < R^2 < 0.9$).

All these equations are suitable for multilayer adsorption of adsorbate onto the adsorbent. In particular, the fitting of these equations can be seen in hetero-porous solids [48]. Conversely, this situation may imply the probability of adsorption of aggregated ions onto the adsorbent surface because the probability of multilayer adsorption for this system is weak. Like Freundlich isotherm model, the Temkin isotherm model considers the interactions between the adsorbed molecules on adsorptive sites, assuming that the adsorption heat of all molecules decreases linearly when the layer is covered and that the adsorption has a maximum energy distribution of uniform bond. A plot of q_e versus $\ln C_e$ enables to tabulate Temkin isotherm constants, which are shown in Table 7. As shown, b_T and a_T are constants related to the heat of adsorption and equilibrium binding constant corresponding to the maximum binding energy, respectively [49]. The obtained values for a_T and b_T are exhibited in Table 7. Based on the obtained correlation coefficient for Temkin model, the

adsorption of AO7 onto CTAB modified MMT is characterized by a uniform distribution of binding energies up to some maximum binding energy and the increasing of temperature probably leads to changing of uniformity [49,50]. The D–R model was used to determine the characteristic porosity and the apparent free energy of the adsorption process. The linear form of D–R isotherm model is as Eq. (11) [44,51]:

$$\ln q_e = K\varepsilon^2 + \ln q_{D-R} \quad (11)$$

where q_e is the amount of adsorbed dye at equilibrium concentration (mg/g), q_{D-R} is D–R maximum adsorption capacity (mg/g), K is the D–R constant (mol^2/J^2) and ε is the Polanyi potential which can be calculated through Eq. (12):

$$\varepsilon = RT \ln(1 + 1/C_e) \quad (12)$$

where C_e is the equilibrium concentration of the dye (mg/L), R is the gas constant (8.314 J/mol K), and T is the temperature (K). The D–R constant (K) can give valuable information about the mean energy of adsorption and estimation of the mechanisms of the adsorption process using Eq. (13):

$$E = 1/(-2k)^{0.5} \quad (13)$$

where E is the mean adsorption energy. The magnitude of E arranged as $E > 8$ kJ/mol and $E < 8$ kJ/mol propose that the adsorption is chemical or physical interaction, respectively. As can be seen from Table 7, the values of E were found to be lower than 8 kJ/mol for all of the studied temperatures, demonstrating that the adsorption of AO7 onto CTAB modified nano-MMT occurs through physical interactions [52].

4. Conclusions

In the present investigation, the application of surfactant modified nano-sized montmorillonite was considered for the adsorption of a textile dye in aqueous phase. The results indicated rapid removal of dye from aqueous solution within 10 min where the cation exchange capacity (CEC) of the modified MMT nanomaterial was 1.0 CEC of pure MMT nanomaterial. To optimize the operational parameters influencing dye removal, central composite design based on the numerical optimization was applied. The maximum decolorization efficiency of 87.19% was predicted at an AO7 concentration of 49 mg/L, adsorbent dosage of 0.8 g/L, reaction time of 27 min and initial pH of 6. Additionally, the results of isotherm study showed that all of the studied model can be suitable for describing the adsorption of AO7 onto the modified MMT except for Langmuir and BET models. Based on the obtained mean adsorption energy (E) of D-R model, the adsorption of AO7 onto modified MMT nanomaterial occurs through a physical interaction especially at low temperatures.

Acknowledgments

The authors thank the University of Tabriz (Iran), Atatürk University of Erzurum (Turkey) and Arak University of Medical Sciences (Iran) for all of the support provided. The third author gratefully acknowledges the International Relations Division Exchange Students Desk, University of Bologna (Italy) for all the support provided.

References

- [1] Karaca S, Gürses A, Açıkyıldız M, Ejder M. Adsorption of cationic dye from aqueous solutions by activated carbon. *Microporous Mesoporous Mater* 2008;115:376–82.
- [2] Rezaee A, Masoumbeigi H, Soltani RDC, Khataee AR, Hashemiyani S. Photocatalytic decolorization of methylene blue using immobilized ZnO nanoparticles prepared by solution combustion method. *Desalin Water Treat* 2012;44:174–9.
- [3] Gürses A, Karaca S, Doğar Ç, Bayrak R, Açıkyıldız M, Yalçın M. Determination of adsorptive properties of clay/water system: methylene blue sorption. *J Colloid Interface Sci* 2004;269:310–4.
- [4] Karaca S, Gürses A, Açılı Ö, Hassani A, Kırışan M, Yıkılmaz K. Modeling of adsorption isotherms and kinetics of Remazol Red RB adsorption from aqueous solution by modified clay. *Desalin Water Treat* 2013;51:2726–39.
- [5] Gürses A, Doğar Ç, Karaca S, Açıkyıldız M, Bayrak R. Production of granular activated carbon from waste *Rosa canina* sp. seeds and its adsorption characteristics for dye. *J Hazard Mater* 2006;131:254–9.
- [6] Gürses A, Doğar Ç, Yalçın M, Açıkyıldız M, Bayrak R, Karaca S. The adsorption kinetics of the cationic dye, methylene blue, onto clay. *J Hazard Mater* 2006;131:217–28.
- [7] Gupta N, Kushwaha AK, Chattopadhyaya MC. Adsorption studies of cationic dyes onto Ashoka (*Saraca asoca*) leaf powder. *J Taiwan Inst Chem Eng* 2012;43:604–13.
- [8] Silva MMF, Oliveira MM, Avelino MC, Fonseca MG, Almeida RKS, Silva Filho EC. Adsorption of an industrial anionic dye by modified-KSF-montmorillonite: evaluation of the kinetic, thermodynamic and equilibrium data. *Chem Eng J* 2012;203:259–68.
- [9] Gürses A, Karaca S, Açıkyıldız M, Ejder M. Thermodynamics and mechanism of cetyltrimethylammonium adsorption onto clayey soil from aqueous solutions. *Chem Eng J* 2009;147:194–201.
- [10] Guerra DJL, da Silva RAR. Kinetic and thermodynamic studies of Brazilian illite-kaolinite in natural and intercalated forms as adsorbents to removal of Zn^{2+} from aqueous solutions. *J Taiwan Inst Chem Eng* 2014;45:268–74.
- [11] Wang L, Wang A. Adsorption properties of Congo Red from aqueous solution onto surfactant-modified montmorillonite. *J Hazard Mater* 2008;160:173–80.
- [12] Gürses A, Karaca S, Aksakal F, Açıkyıldız M. Monomer and micellar adsorptions of CTAB onto the clay/water interface. *Desalination* 2010;264:165–72.
- [13] Darvishi Cheshmeh Soltani R, Rezaee A, Godini H, Khataee AR, Hasanbeiki A. Photoelectrochemical treatment of ammonium using seawater as a natural supporting electrolyte. *Chem Ecol* 2013;29:72–85.
- [14] Darvishi Cheshmeh Soltani R, Rezaee A, Khataee AR, Godini H. Optimisation of the operational parameters during a biological nitrification process using response surface methodology. *Can J Chem Eng* 2013;92:13–22.
- [15] Khataee AR, Dehghan G. Optimization of biological treatment of a dye solution by macroalgae *Cladophora* sp. using response surface methodology. *J Taiwan Inst Chem Eng* 2011;42:26–33.
- [16] Khataee AR, Zarei M, Moradkhannejhad L. Application of response surface methodology for optimization of azo dye removal by oxalate catalyzed photo-electro-Fenton process using carbon nanotube-PTFE cathode. *Desalination* 2010;258:112–9.
- [17] Sharma P, Singh L, Dilbaghi N. Response surface methodology approach for the decolorization of simulated dye effluent using *Aspergillus fumigatus* fresenius. *J Hazard Mater* 2009;161:1081–6.
- [18] Silva JP, Sousa S, Gonçalves I, Porter JJ, Ferreira-Dias S. Modelling adsorption of acid orange 7 dye in aqueous solutions to spent brewery grains. *Sep Purif Technol* 2004;40:163–70.
- [19] Darvishi Cheshmeh Soltani R, Rezaee A, Khataee AR, Safari M. Photocatalytic process by immobilized carbon black/ZnO nanocomposite for dye removal from aqueous medium: optimization by response surface methodology. *J Ind Eng Chem* 2013;20:1861–8.
- [20] Czimmerová A, Bujdák J, Dohmann R. Traditional and novel methods for estimating the layer charge of smectites. *Appl Clay Sci* 2006;34:2–13.
- [21] Madeira M, Auxtero E, Sousa E. Cation and anion exchange properties of Andisols from the Azores, Portugal, as determined by the compulsive exchange and the ammonium acetate methods. *Geoderma* 2003;117:225–41.
- [22] Yang H, Zheng X, Huang W, Wu K. Modification of montmorillonite with cationic surfactant and application in electrochemical determination of 4-chlorophenol. *Colloids Surf B* 2008;65:281–4.
- [23] Karaca S, Gürses A, Ejder Korucu M. Investigation of the orientation of CTA⁺ ions in the interlayer of CTAB pillared montmorillonite. *J Chem* 2013;2013:10.
- [24] Kousha M, Daneshvar E, Sohrabi MS, Koutabzadeh N, Khataee AR. Optimization of C.I. Acid black 1 biosorption by *Cystoseira indica* and *Gracilaria persica* biomasses from aqueous solutions. *Int Biodeter Biodegrad* 2012;67:56–63.
- [25] Bessekhouad Y, Robert D, Weber JV, Chaoui N. Effect of alkaline-doped TiO₂ on photocatalytic efficiency. *J Photochem Photobiol A* 2004;167:49–57.
- [26] Singh KP, Gupta S, Singh AK, Sinha S. Optimizing adsorption of crystal violet dye from water by magnetic nanocomposite using response surface modeling approach. *J Hazard Mater* 2011;186:1462–73.
- [27] Vargas AMM, Martins AC, Almeida VC. Ternary adsorption of acid dyes onto activated carbon from flamboyant pods (*Delonix regia*): analysis by derivative spectrophotometry and response surface methodology. *Chem Eng J* 2012;19:5–196. 173–9.
- [28] Cazetta AL, Junior OP, Vargas AMM, da Silva AP, Zou X, Asefa T, et al. Thermal regeneration study of high surface area activated carbon obtained from coconut shell: characterization and application of response surface methodology. *J Anal Appl Pyrolysis* 2013;101:53–60.
- [29] Tang J, Yang ZF, Yi YJ. Enhanced adsorption of methyl orange by vermiculite modified by cetyltrimethylammonium bromide (CTMAB). *Proc Environ Sci* 2012;13:2179–87.
- [30] Pan J, Guan B. Adsorption of nitrobenzene from aqueous solution on activated sludge modified by cetyltrimethylammonium bromide. *J Hazard Mater* 2010;183:341–6.
- [31] Ma J, Cui B, Dai J, Li D. Mechanism of adsorption of anionic dye from aqueous solutions onto organobentonite. *J Hazard Mater* 2011;186:1758–65.
- [32] Mandatia T, Bergaya F. Organo clay mineral-melted polyolefin nanocomposites: effect of surfactant/CEC ratio. *J Phys Chem Solids* 2006;67:836–45.
- [33] Zohra B, Aicha K, Fatima S, Nouredine B, Zoubir D. Adsorption of Direct Red 2 on bentonite modified by cetyltrimethylammonium bromide. *Chem Eng J* 2008;136:295–305.
- [34] Haber A, Runyun R. General statistics. Boston, MA: Addison-Wesley; 1977.
- [35] Khataee AR, Zarei M, Asi SK. Photocatalytic treatment of a dye solution using immobilized TiO₂ nanoparticles combined with photoelectro-Fenton process: optimization of operational parameters. *J Electroanal Chem* 2010;648:143–50.
- [36] Hamzeh Y, Ashori A, Azadeh E, Abdulkhani A. Removal of Acid Orange 7 and Remazol Black 5 reactive dyes from aqueous solutions using a novel biosorbent. *Mater Sci Eng C* 2012;32:1394–400.
- [37] Mana M, Ouali MS, de Menorval LC, Zajac JJ, Charnay C. Regeneration of spent bleaching earth by treatment with cetyltrimethylammonium bromide for application in elimination of acid dye. *Chem Eng J* 2011;174:275–80.
- [38] Darvishi Cheshmeh Soltani R, Khataee AR, Safari M, Joo SW. Preparation of bio-silica/chitosan nanocomposite for adsorption of a textile dye in aqueous solutions. *Int Biodeter Biodegrad* 2013;85:383–91.
- [39] Selvam PP, Preethi S, Basakaralingam P, Thinakaran N, Sivasamy A, Sivanesan S. Removal of rhodamine B from aqueous solution by adsorption onto sodium montmorillonite. *J Hazard Mater* 2008;155:39–44.
- [40] Alkan M, Doğan M. Adsorption kinetics of Victoria blue onto perlite. *Fresenius Environ Bull* 2003;12:418–25.
- [41] Asfour HM, Fadafi OA, Nassar MM, El-Geundi MS. Equilibrium studies on adsorption of basic dyes on hardwood. *J Chem Technol Biotechnol A* 1985;35:21–7.
- [42] Bouberka Z, Kacha S, Kameche M, Elmaleh S, Derriche Z. Sorption study of an acid dye from an aqueous solutions using modified clays. *J Hazard Mater* 2005;119:117–24.
- [43] Hameed BH, Ahmad AA, Aziz N. Isotherms, kinetics and thermodynamics of acid dye adsorption on activated palm ash. *Chem Eng J* 2007;133:195–203.
- [44] Darvishi Cheshmeh Soltani R, Shams Khorramabadi GH, Khataee AR, Jorfi S. Silica nanopowders/alginate composite for adsorption of lead (II) ions in aqueous solutions. *J Taiwan Inst Chem Eng* 2013;45:973–80.
- [45] Alver E, Metin AU. Anionic dye removal from aqueous solutions using modified zeolite: adsorption kinetics and isotherm studies. *Chem Eng J* 2012;200–202:59–67.
- [46] Rosen MJ. Surfactants and interfacial phenomena. USA: John Wiley & Sons, Inc.; 1978.

- [47] Gimbert F, Morin-Crini N, Renault F, Badot P-M, Crini G. Adsorption isotherm models for dye removal by cationized starch-based material in a single component system: error analysis. *J Hazard Mater* 2008;157:34–46.
- [48] Karaca S, Gürses A, Bayrak R. Investigation of applicability of the various adsorption models of methylene blue adsorption onto lignite/water interface. *Energy Convers Manag* 2005;46:33–46.
- [49] Temkin Mf, Pyzhev V. Recent modifications to Langmuir isotherms. *Acta Physicochim URSS* 1940;12:217–22.
- [50] Zhou L, Jin J, Liu Z, Liang X, Shang C. Adsorption of acid dyes from aqueous solutions by the ethylenediamine-modified magnetic chitosan nanoparticles. *J Hazard Mater* 2011;185:1045–52.
- [51] Santhana Krishna Kumar A, Ramachandran R, Kalidhasan S, Rajesh V, Rajesh N. Potential application of dodecylamine modified sodium montmorillonite as an effective adsorbent for hexavalent chromium. *Chem Eng J* 2012;211–212:396–405.
- [52] Foo KY, Hameed BH. Insights into the modeling of adsorption isotherm systems. *Chem Eng J* 2010;156:2–10.